Iron Carbides: Control Synthesis and Catalytic Applications in CO_x Hydrogenation and Electrochemical HER

*Siwei Li, Jinghe Yang, Chuqiao Song, Qingjun Zhu, Dequan Xiao, and Ding Ma**

S. Li, C. Song, Prof. D. Ma.
Beijing National Laboratory for Molecular Sciences, College of Chemistry and Molecular Engineering and College of Engineering, and BIC-ESAT, Peking University, Beijing 100871, P. R. China.
E-mail: dma@pku.edu.cn

Dr. J. Yang
School of Chemical Engineering and Energy, Zhengzhou University, Zhengzhou 450001, P. R. China.

Dr. Q. Zhu
Fritz-Haber-Institut der Max-Planck-Gesellschaft, Faradayweg 4-6, D-14195 Berlin, Germany

Prof. D. Xiao
Center for Integrative Materials Discovery, Department of Chemistry and Chemical Engineering, University of New Haven, West Haven, CT 06516

Keywords: (iron carbides, control synthesis, Fischer-Tropsch synthesis, CO_2 hydrogenation, HER)

Abstract. Catalytic transformation of CO_x (x=1,2) with renewable H_2 into valuable fuels and chemicals provides practical processes to mitigate the worldwide energy crisis. Fe-based catalytic materials are widely used for those reactions due to their abundance and low cost. Novel iron carbides are particularly promising catalytic materials among the reported ferrous catalysts. Recently, a series of strategies are developed for the preparations of the iron carbide nanoparticles and their nanocomposites. Herein, we review the control synthesis of FeC_x-based nanomaterials and their catalytic applications in CO_x hydrogenation and electrochemical hydrogen evolution reaction (HER). The discussion is focused on the unique catalytic activities of iron carbides in CO_x hydrogenation and HER as well as the correlation between structure and catalytic performance. Future synthesis and potential catalytic applications of iron carbides are summarized at the end of this research progress.

1. Introduction

Transportation fuels are normally produced from petroleum. The rapid consumption of petroleum has triggered growing enthusiasm to search for alternative fuels or new energy-carriers.[1] Among these approaches, Fischer-Tropsch synthesis (FTS), which transforms coal/biomass/shale gas derived syngas (CO and H_2) into liquid fuels and high-value chemicals, plays an important role in academic and industry.[2-11] Meanwhile, catalytic hydrogenation of CO_2 is very attractive because it not only produces useful chemicals and fuels, but also recycles the CO_2 generated from industrial processes, which can eventually lead to the reduction of atmospheric CO_2.[12, 13] The transformation of these CO_x (x=1,2) feedstocks requires the participating of H_2 molecules. Besides H_2 generated from fossil fuel feedstocks, renewable H_2 produced from electrochemical HER using the electricity from renewable energy sources (e.g., solar, wind, or nuclear energy) in CO_x conversion is promising.[14-16] Thus, CO_x hydrogenation and electrochemical HER are two essential reactions to develop the next-generation technology of liquid fuel production.

Iron carbide is an ancient material. The bulk Fe_3C was found in Wootz steel, a 2500-year-old material in India, which was largely used for daggers and swords because of its superior lightness and hardness. In the past few years, the catalytic application of this ancient material has drawn growing interest. Iron carbides are of great potentials for both CO_x hydrogenation and HER process in industry, because iron is an earth-abundant element. Specifically, FeC_x was considered as the active phase in the Fe-based FTS reaction.[17-24] Varieties of useful products such as liquid fuels, alkenes, alcohols, and aromatics were obtained with high selectivity over modulated iron carbides catalysts.[25-27] Moreover, the ferrous mixture containing FeO_x and Fe_5C_2 was a robust catalyst for the production of valuable C_{2+} species through CO_2 hydrogenation reactions.[28] Furthermore, the FeC_x with high Fe content (e.g., Fe_3C and Fe_3C/Fe) exhibited impressive catalytic performance in electrochemical reactions including hydrogenation evolution reaction,[29, 30] oxygen reduction reaction,[31-36] and CO_2 reduction reaction.[37]

Despite the wide applications of iron carbides, the research on them is still limited compared to metallic iron or iron oxides, largely due to the obstacles in FeC_x synthesis. For example, the control of crystal phase, particle size, morphology, and composition (the critical factors for catalysis) in FeC_x synthesis remains as a great challenge. Recently, novel preparation routes such as sol-gel methods,[38] solid-state reaction methods[39] and wet-chemical methods[17] have been developed for iron carbides. Pure-phase FeC_x was successfully synthesized, and the particle size of FeC_x nanoparticles (NPs) could be controlled in some reports.[40] The synthesis of pure-phase FeC_x has led to in-depth understanding of the reaction mechanisms in CO_x hydrogenation and electrocatalytic HER. In this report, we focus on reviewing recent progress in control synthesis of FeC_x-based materials and their catalytic performances in CO_x hydrogenation and electrochemical HER.

2. Structures and Properties of Iron Carbides

Iron carbide is one type of intermetallic compounds that carbon atoms occupy the interstices between close-packed iron atoms. As shown in the Fe-C phase diagram (see Figure 1), changing the carbon content results in the change of the crystal phase and structure of iron carbides.[41] According to the location of carbon atoms, FeC_x can be further classified as octahedral interstices ($Fe_{2.2}C$ and Fe_2C) or trigonal-prismatic interstices (Fe_7C_3, Fe_5C_2 and Fe_3C). From the view point of thermodynamics, the cementite Fe_3C is stable among these different phases whereas the Fe_5C_2 and Fe_2C are meta-stable.[40]

The introduction of carbon atoms to Fe atoms in FeC_x influences the physical and chemical properties of the material. Compared to pure iron, bulk FeC_x is resistant against chemical corrosion (e.g., water and oxygen). However, the surface of FeC_x NPs is sensitive to oxidative atmosphere. Once exposed to air, the FeC_x surface is easily coated with FeO_x shell.[17, 42] FeC_x was reported to possess outstanding magnetism,[43, 44] and high adsorption of near

infrared (NIR) light [45-47] due to the presence of carbon atoms. As a consequence, electromagnetic or solar energy can be efficiently converted into heat over FeC_x.

3. Control Synthesis of Iron Carbides

As discussed above, control synthesis of iron carbides is challenging. In this section, we focus on the synthetic methods of FeC_x that were widely used in heterogeneous catalysis including sol-gel methods, solid-state reaction methods, and wet-chemical synthetic methods.

3.1 Sol-Gel Methods

The sol-gel methods involve hydrolysis and condensation of metallic alkoxides, in which the reactants can be mixed at the molecular level. Giordano et al. developed a simple "urea glass route" for the preparation of various transition metal carbides and nitrides.[48, 49] The key feature of this strategy is the formation of a gel-like/glassy precursor constituting of a polymeric complex containing organic amine and the metal precursor. When applied to the iron carbide system, the gel was prepared by slowly adding urea into the ethanol solution of $FeCl_2$ and $Fe(CO)_5$ precursor. The gel was then heated under N_2 at 700 ^oC for 2 hours, leading to the formation of small Fe_3C NPs (about 10 nm in size) via carbothermal reduction.[38] Moreover, mesoporous Fe_3C sponges with high specific surface areas (415 m^2/g) were further synthesized through combination of the urea glass route and hard template strategy.[50] Owing to the extremely large specific surface areas, the mesoporous Fe_3C sponges exhibited high activity towards ammonia decomposition reaction. However, the iron carbide was not stable under the reaction condition of ammonia decomposition and would be fully converted to iron nitride. In the urea glass route, urea can also be replaced by a biopolymer (e.g., gelatin) to get a stand-alone gel precursor.[43] The sol-gel method has the advantage in large-scale preparation of homogeneous FeC_x NPs with small particle size, although the phases other than Fe_3C has not yet been synthesized via this method.

3.2. Solid-State Reaction Methods

Solid-state reaction methods are common strategies for preparing transition metal carbides (TMCs), which usually involve high-temperature solid-gas or solid-solid reactions between metal and carbon sources.[51] The phase of FeC_x could be determined by a variety of parameters such as reaction precursor, temperature, atmosphere, pressure, and the flow rate of carrier gas. Generally speaking, FeC_x with high C content (e.g., Fe_2C and Fe_5C_2) could be formed in the CO or syngas atmosphere, because of the gas's strong capability for the reduction and carburization of Fe precursors.[52, 53] The synthesis of pure-phase Fe_5C_2 was firstly reported by Tajima et al. via the reaction of iron oxides and carbon monoxide. By controlling the reaction temperature and precursor, Fe_3O_4 was confirmed as the intermediate of Fe_5C_2 under this reaction condition.[39] β-Fe_2O_3 was used as the starting material and its temperature evolution carburization process in CO atmosphere was investigated.[54] It was found that Fe_3C and Fe_5C_2 were the dominant phases at 625 ºC and 700 ºC, respectively. Hensen et. al synthesized pure-phase Fe_2C by carefully controlling the pretreatment and carburization processes (see Figure 2a).[55] It was concluded that the precursor must be completely reduced to metallic Fe, otherwise the products could become a mixture of iron carbides and oxides, because Fe_3O_4 could not be carburized under the synthesis gas ($H_2/CO/N_2$) at 250 ºC.

Carbon-rich organic and carbon nanomaterials could be used as solid carbon sources, which result in the generation of Fe_3C, a type of FeC_x with the lowest carbon content.[56, 57] The Fe_3C/C hollow spheres were synthesized via a high-pressure pyrolysis of ferrocene and cyanamide at 700 ºC in N_2.[57] The carbon shell could protect Fe_3C NPs from acid corrosion without depriving their electrocatalytic activity. In contrast, bamboo-like carbon nanotube/Fe_3C nanohybrids were reported in a one-pot synthesis by annealing a mixture of $Fe(NO)_3$, EG-PPG-PEG (P 123) and melamine at 800 ºC in N_2 (Figure 2d-e).[58] It is noted

that temperature is the key factor for bamboo-like structure. Low temperatures (e.g., 700 ºC) led to carbon nanoshell (Figure 2c) whereas high temperatures (e.g., 900 or 1000 ºC) resulted in the formation of irregular NPs. In general, the solid-state reaction methods have the advantage of easy operation. However, the reaction condition must be carefully controlled to prepare pure-phase FeC_x NPs.

3.3. Wet-Chemical Synthetic Methods

Wet-chemical synthetic strategies are known for the control of composition and morphology of expected nanostructures.[59, 60] In a typical wet-chemical synthesis process of iron carbides, metal precursors were introduced into a solution of solvent, surfactant, and inducing agents under a mild temperature and atmosphere. The reaction mixture may be heated to a high temperature for the crystal growth and carburization of FeC_x NPs. The monodispersed FeC_x (mixture of $Fe_{2.2}C$ and Fe_5C_2) and core-shell Fe/FeC_x NPs were synthesized.[61] Reaction temperature and atmosphere affected the amount of carbon that was formed and diffused into the Fe NPs, and finally determined the phase and composition of products. The work by Chaudret et al.[61] is pioneering, however, unable to fabricate pure-phase FeC_x NPs.

The wet-chemical synthetic method has been remarkably developed for pure-phase Fe_5C_2 NPs by Hou et al. recently.[17] Typically, $Fe(CO)_5$ and Br^- were used as iron source and inducing agent, respectively. Octadecylamine (ODA) was employed as the solvent, surfactant and carbon source. TEM and HR-TEM images (Figures 3a-b) showed that the Fe_5C_2 NPs were about 20 - 50 nm in size without agglomeration due to mild reaction conditions (e.g., 350 ºC). XRD together with EXAFS results confirmed the generation of pure-phase Fe_5C_2. More importantly, the one-pot synthetic method could be further employed to produce Co_2C and MoC NPs.[62, 63]

In order to reveal the formation mechanism of pure-phase Fe_5C_2, a number of in-situ characterization techniques were utilized to study the details of this synthetic reaction in the gas, liquid, or solid phase (Figure 3c).[62] As shown in Figure 3d, the entire synthetic procedure could be divided into 4 steps: 1) precursor decomposition (at 180 - 215 ºC), 2) nucleation and growth of FeO NPs (at 215 - 270 ºC), 3) reduction of FeO NPs to Fe NPs (at 270 - 300 ºC), and 4) carburization of Fe NPs to Fe_5C_2 NPs (at 300 - 350 ºC). Fe species in the reaction mixture could catalyze the dehydrogenation and cracking reactions of ODA, which is responsible for the formation of Fe_5C_2 NPs. GC-MS and FTIR showed that ODA was converted to nitrile and absorbed on the surface of as-synthesized Fe_5C_2. The mechanism of wet-chemical synthesis of Fe_5C_2 NPs was clearly illustrated by the complementary in-situ techniques.

The seeded-growth method was further developed for controlling the phase and size of FeC_x.[64] First of all, bcc-Fe NPs were synthesized and oxidized to $Fe@Fe_3O_4$ core-shell nanostructures (see Figure 4a). Homogeneous Fe_3O_4 shell was critical for the size control of iron carbide NPs because the Fe_3O_4 phase could not be transformed under the synthetic condition. It was suggested that inducing agents were unnecessary for the formation of Fe_2C (Figure 4b), as it is the thermodynamically favorable phase at low temperatures. The pure phase Fe_5C_2 and Fe_3C NPs were prepared in the same procedure except for the introduction of different amounts of Cl^- ions (see Figures 4c-d). The adsorption of Cl^- ions on the iron could weaken Fe-C bonds, which hindered the penetration of carbon atoms and facilitate the formation of iron carbide NPs with lower carbon content (Figure 4e). Apparently, these pure-phase iron carbide NPs with tunable particle sizes have great potentials in catalytic applications.

By the wet-chemical synthetic methods, iron carbides with different phases could be prepared under similar conditions, which led to reasonable comparison of the catalytic performances of different FeC_x. The strong interaction between iron and halide ions is

important for the formation of distinct phase of iron carbides. Moreover, FeC_x-based bimetallic materials can be designed by understanding the synthetic chemistry. Co-carburization of metal precursors led to the formation of alloy carbides. For example, $(Fe_xCo_{1-x})_5C_2$ NPs were synthesized when $Co_2(CO)_8$ and $Fe(CO)_5$ were introduced simultaneously into the reaction mixture.[65] In addition, secondary growth through decomposition or reduction of the metal precursor on as-synthesized iron carbides NPs led to a core-shell or core-satellite structure of FeC_x-M. Fe_5C_2-Co and $Fe_{2.2}C$-Ni hybrid catalysts have been fabricated with this strategy.[66, 67] Clearly, the wet-chemical synthetic strategies meet the demands for FeC_x synthesis in laboratory. We anticipate that many important issues in heterogeneous catalysis could be addressed using the phase- and size-controlled FeC_x NPs in the near future.

4. Applications of FeC_x for CO_x Hydrogenation and Electrochemical HER

One of the most important applications of FeC_x materials are for the catalysts in CO_x hydrogenation and electrochemical HER. In the followings, we will discuss the unique catalytic activities of FeC_x.

4.1. Thermal Catalytic FTS Process

Fe-based FTS catalysts have attracted extensive interest due to the low cost, high activity, and good selectivity control.[7, 25, 26] Syngas could be converted to valuable products including α-olefin, aromatic compounds and alcohols over Fe-based catalysts. Despite the outstanding catalytic performance of Fe-based FTS catalyst, there are debates concerning the nature of the active phase.

Fe_5C_2 is the most widely recognized active phase in Fe-based FTS catalysts.[25, 68, 69] One reason is that, under the reaction condition of conventional Fe-based FTS (e.g., 270 ~ 340 ºC , 3.0 ~ 5.0 MPa), Fe_5C_2 is likely to be the most thermodynamically favored phase among all of possible FeC_x.[70] The Fe_5C_2 NPs can catalyze the conversion of syngas to

hydrocarbons without activation, as evidenced by a temperature programmed surface reaction (TPSR) up to 270 ºC (see Figures 5a-b), which pinpoints Fe_5C_2 as the intrinsic active phase of Fe-based FTS. Impressively, Fe_5C_2 exhibited a selectivity of 55% and initial activity of 40% towards value-added products (e.g., C_2-C_4 olefin and C_{5+} hydrocarbons), which are in sharp contrast to those of conventional reduced Fe catalysts (with 35% in selectivity 18% in activity). After running the reaction for 100 hours, the Fe_5C_2 catalysts deactivated to 55% of its initial activity. XRD results showed that the Fe_5C_2 kept as the major phase except for the formation of Fe_3O_4, suggesting the deactivation is due to the oxidation to Fe_3O_4 by CO_2 and H_2O produced in-situ.

Fe_3C is identified as an inactive phase for FTS since it mainly appeared in the deactivated Fe-based FTS catalysts.[71, 72] Fe_2C is considered as an active phase at low temperature and/or low H_2/CO ratios FTS process.[73-76] Hensen et al. examined the FTS catalytic activity of pure-phase Fe_2C catalysts which exhibited stable FT performance at 235 °C and 23 bar for 150 hours and showed extremely low selectivity towards CO_2 formation (see Figure 2b).[55] In addition, Fe_7C_3 phase existed in a long-term FTS process, and was demonstrated to be active for middle-temperature (MT) FTS.[77] Furthermore, iron carbides with different composition (e.g., Fe_5C_2, Fe_2C+Fe_5C_2, and Fe_7C_3+Fe_5C_2) were obtained in the Fe/SiO_2 catalyst system by varying the pretreatment methods. Theoretical calculations suggested that Fe_7C_3 had the highest activity among three iron carbides candidates in the MT-FTS process.

As Fe_5C_2, Fe_2C and Fe_7C_3 are identified to be active in different reports, great efforts have been devoted to investigate the catalytic performance of different phases of FeC_x. However, the iron carbides in these reports were significantly different in size, which also have impacts on the FTS activity. Thus, the comparisons between different reports are not suitable. Furthermore, the phase transformation under FTS conditions makes it difficult to explore the instinct activity of a pure-phase iron carbide catalyst. It is proposed that multiple

pure-phase size-controlled FeC_x NPs could be prepared via the wet-chemical synthesis strategy, which could be utilized to identify the most active phase of FeC_x and investigate the size effect in Fe-based FTS reactions.

Fe_5C_2/Co heterostructure materials were fabricated, upon the synthesis of pure-phase Fe_5C_2, which exhibited a high activity and excellent stability toward low temperature FTS (Figure 6).[66] Among the two major categories of FTS catalysts (i.e., Fe and Co based catalysts), iron-based catalysts are cheaper.[78-80] In contrast, cobalt-based catalysts, though five hundred times more expensive than iron-based catalysts, are usually more stable and active. [81-85] Therefore, a suitable combination of Fe and Co sites is highly desired. With the as-synthesized Fe_5C_2 NPs as the substrate, metallic Co NPs could be grown through the second-growth strategy to obtain hybrid catalysts. It was found that the 7 wt% Fe_5C_2/Co, though with only 0.6 wt% of Co incorporated, exhibited the same activity as that of the 7 wt% conventional impregnated Co catalyst at 220 ºC, and was four times more active than the original Fe_5C_2 catalyst. Pulse reaction of CO and syngas revealed that the outstanding catalytic performance of Fe_5C_2/Co catalyst originated from its "dual center" characteristics, i.e., the Co site promoted the dissociation of CO while the Fe_5C_2 site dominated the chain propagation.[66] At low temperatures (i.e., 220 ºC, Cobalt FTS temperature), Fe_5C_2 was barely active for CO activation, while remained its activity for C-C coupling. Therefore, with the decoration of the active phase metallic cobalt, CO was dissociated to C_1 species under low temperature and migrated to the Fe_5C_2 sites to form longer chain hydrocarbons as evidenced by the pulse reaction experiment. This proved that Fe_5C_2 is an effective platform to design new FTS catalysts, where the effect of support and additive can be studied.

4.2 Thermal Catalytic CO_2 Hydrogenation

Among the products of CO_2 hydrogenation, C_{2+} species can serve as the entry platform to produce other valuable chemicals and therefore offer more advantages than C_1 species.[86]

Hydrogenation of CO_2 to C_{2+} products through FTS routes involves the initial process of producing carbon monoxide by reverse water gas shift reaction (RWGS, $CO_2 + H_2 = CO + H_2O$) followed with hydrogenation of the CO intermediate.[87] Fe-based catalyst is one of the most important candidates for obtaining C_{2+} products via CO_2 hydrogenation.[88] Usually, FeO_x are used as catalysts for the RWGS reaction. In this process, FeC_x can be formed in-situ, leading to the hydrogenation of CO intermediate into C_{2+} products.[89-91]

The K-promoted Fe_3O_4/γ-Fe_2O_3 precursor was prepared and treated by carburization in syngas at 350 ºC, leading to a mixture of Fe_3O_4, Fe_5C_2 and metallic Fe.[92] This catalyst exhibited high selectivity to lower olefins at mild conditions (e.g., 300 °C and 0.5 MPa). It was proposed that the proper ratio of Fe_3O_4 to Fe_5C_2 resulted in a modest chain growth, and the potassium species on the surface acted as an electronic promoter and suppressed the hydrogenation of olefins, resulting in high selectivity towards C_2-C_4 olefins. As shown in Figure 7, CO_2 was converted into gasoline-range hydrocarbons (C_5-C_{11}) with a selectivity of 78% towards all hydrocarbons, and only 4% CO_2 was transformed to CH_4 at the conversion of 22% over the Na-Fe_3O_4/HZSM-5 catalyst.[28] Clearly, HZSM-5 provided acid sites to catalyze isomerization, oligomerization and aromatization reactions of α-olefins intermediates. As evidenced by these results, both iron oxides and carbides are indispensable for the formation of C_{2+} products. FeO_x, without the promotion of the secondary metal, leads to low content of FeC_x and thus low selectivity towards C_{2+} product.

4.3 CO_x Hydrogenation Driven by Renewable Energy

In CO_x hydrogenation, it is noticed that most industrial catalysts need to work under a relatively harsh reaction conditions especially for high temperature and high pressure to maintain an acceptable yield,[93] leading to high energy consumption.[94] Therefore, novel sustainable and green solutions to drive the FTS and CO_2 hydrogenation reactions are highly

desirable. Excellent photothermal and magnetothermal effects of FeC_x offer the opportunity to heat the catalytic CO_x reaction using sustainable energy.[46, 95]

Sunlight is the most ubiquitous and abundant energy source for hydrocarbon cycling on earth. Compared to the traditional thermal catalytic process, photo-driven CO_x transformation provides a sustainable approach to harvest the most abundant energy in nature to obtain desired fuels and chemicals.[96, 97] Recently, a novel photo-driven FT to olefins process was realized over Fe_5C_2 catalyst, which showed an olefin/paraffin (o/p) ratio of 10.9 under the CO conversion of ~49% as well as low CO_2 selectivity (18.9%) (Figure 8a).[42] Significantly different product distributions were observed under photo-driven and thermal reactions. The surface of Fe_5C_2 NPs was decorated partly by O atoms under solar irradiation, which modulated the optical band gap and local electronic structure of the catalyst, leading to readily assessable C_2H_4 desorption and thus high selectivity to olefins. More importantly, the catalytic activity and selectivity were kept almost intact within 5 runs of the reaction. The authors further employed in-situ EXAFS to demonstrate that Fe_5C_2 was very stable under the low-temperature photo-irradiation condition. In contrast, the Fe_5C_2 surface was heavily oxidized after traditional thermal FTS reaction, resulting in poor catalytic performance and deactivation of iron carbides. This strategy provides a new sustainable route for the activation and selective conversion of CO into valuable chemicals over iron carbides.

Magnetism-induced thermal heating has the advantages of short warming time and high heating efficiency. Kirschning et al. proposed the concept of magnetically induced catalysis by applying iron oxide NPs in numerous chemical reactions in liquid media.[98, 99] Magnetism-induced CO_x hydrogenation reaction utilizes the heating energy in an effective way. On the other hand, the process could also be viewed as the storage of electric or electromagnetic energy into chemicals. The magnetothermal FTS process was performed in a closed vessel over core−shell Fe@Ru and Fe@FeCo nanoobjects. Recently, a magnetically induced CO_2 methanation reaction with 93% selectivity to CH_4 was developed in a

continuous-flow reactor (Figure 8b) over FeC_x@Ni NPs that was loaded on the ruthenium modified $SiRAlO_x$ support.[67] Iron carbide NPs with over 80% crystalline $Fe_{2.2}C$ exhibited excellent magnetothermal property but poor catalytic reactivity in magnetism-induced CO_2 hydrogenation reaction. CO_2 conversion and CH_4 selectivity were drastically enhanced by the deposition of Ni on iron carbide NPs and the use of 1wt % Ru-containing supports (Figure 8c). The conversion efficiencies of electricity to heat reached the high values of 80 - 90%. Although the overall energy storage efficiency is still quite low (1%) due to the lack of optimization, this report offers the possibility to transform electrical or electromagnetic energy into chemicals via magnetism-induced CO_2 hydrogenation.

4.4 Electrochemical HER

Water electrolysis has been applied industrially to produce high-quality CO_x-free H_2.[100] Transition metal carbides such as Mo_xC and W_xC were demonstrated to be robust electrocatalysts.[101-103] Compared to molybdenum or tungsten, iron has significant advantages in cost, but there are few reports about iron carbide-based materials as HER catalysts.[104-106] Indeed, pure-phase iron carbides are not catalytically active for HER as shown by experiments and calculations.[65, 107] Nevertheless, encapsulating iron carbide NPs into carbon nanomaterials is an efficient way to improve the HER catalytic performance and durability. TMCs (M_3C, M= Fe, Co and Ni) were synthesized and encapsulated in graphitic shells, which was supported with vertically aligned graphene nanoribbons (VA-GNRs) via a modified chemical vapor deposition method,[30] and the electrocatalysts exhibited remarkable catalytic performance towards HER. The Fe_3C/VA-GAR electrocatalyst showed the highest HER catalytic activity with the lowest onset overpotential of 32 mV in an acidic solution. In comparison, Fe_3C nanorods encapsulated in N-doped carbon nanotubes (Fe_3C@NCNT) were prepared through the pyrolysis of an iron-based metal organic framework and melamine.[107] Fe_3C@NCNT exhibited a low overpotential of 154 mV at the current density of 10 mA/cm^2.

The DFT calculations showed that the absorption of H_2 on Fe_3C@NCNT is more suitable than that of Fe_3C, leading to a high HER activity.

Doping iron carbides with a second metal is an alternative strategy for enhancing their HER activity. Recently, cobalt-modified Fe_5C_2 NPs were used for catalyzing the HER in an alkaline environment (Figure 9a). Fe_5C_2 exhibited poor catalytic activity with an overpotential of 780 mV, but was significantly enhanced after the introduction of cobalt into the Fe_5C_2 lattice regardless of the content. $(Fe_{0.75}Co_{0.25})_5C_2$ showed the lowest overpotential (174 mV @ 10 mA/cm^2) after the optimization (Figure 9b). Based on DFT calculations, the impact of Co could be summarized into two aspects: 1) the introduced Co sites in $(Fe_{1-x}Co_x)_5C_2$ served as catalytic active sites, 2) carbidic C was activated upon Co doping. XAFS was employed to understand the origin of the activation of carbon sites upon Co introduction. The Fe K-edge XANES spectrum (Figure 9c) showed that Fe species in $(Fe_{0.75}Co_{0.25})_5C_2$ gave out more electrons than those in Fe_5C_2. Accordingly, the C K-edge spectra showed significant enhancement of the electron density in the carbon sites on $(Fe_{0.75}Co_{0.25})_5C_2$, which were widely accepted as active sites for HER. This work not only verified the prediction of poor HER catalytic activity for FeC_x, but also proved the doping effect of a second metal in bimetallic $(Fe_{1-x}Co_x)_5C_2$.

HER is one of the key components in microbial electrolysis cells (MEC), a device for producing high-value energy products from organic waste. By annealing the Fe-based NPs loaded on C_3N_4 and polymers, Chen and He et al. prepared a novel iron carbide-based material, i.e., nitrogen-containing core-shell N-Fe/Fe_3C@C. The N–Fe/Fe_3C@C was used to modify the cathode for catalyzing the hydrogenation reaction in the MEC.[29] Although the catalytic activity of the N–Fe/Fe_3C@C cathode was slightly lower than that of the commercial Pt/C cathode, the price of commercial Pt/C was estimated 20 times more than the iron carbide-based cathode. The simplicity in synthesis and the low-cost makes the iron carbide-based material a promising alternative to commercial Pt/C in MEC.

5. Conclusion and Perspective

Hydrogenation of CO_x into fuels and chemicals using renewable H_2 produced from electrocatalytic HER are of great importance. Recent advances in CO_x hydrogenation and electrocatalytic HER have unambiguously indicated that with the low cost and high catalytic activity, iron carbides and their derived heterostructures are particularly promising for these two reactions in both academia and industry. Remarkable research efforts have been devoted to the control synthesis of iron carbides nanomaterials. A variety of pure-phase iron carbide NPs such as Fe_5C_2, Fe_2C, Fe_3C and $Fe_{2.2}C$ have been successfully prepared via sol-gel methods, solid-state reaction methods and wet-chemical methods. The development in the control synthesis of FeC_x NPs has deepened our understanding of some basic questions in Fe-based catalytic reactions. Although the obstacles in control synthesis have been removed to some extent, there remain fundamental issues to be addressed for CO_x hydrogenation. For example, comparing the initial FTS activity of iron carbides with different crystalline phases can offer clues to identify the most active phase of the Fe-based catalyst. Moreover, controlling the particle size of FeC_x NPs can provide the opportunity to investigate the size effect in Fe-based FTS processes.

Based on the understanding of the unique catalytic properties of iron carbide NPs, FeC_x-based hybrid catalysts have been rationally designed as active species rather than mere trials-and-errors. Technically speaking, the wet-chemical synthesis strategy is particularly powerful for preparing iron carbide based nanocomposites. Understanding the formation mechanism in the wet-chemical synthesis of iron carbide NPs has provided insightful guidance towards the fabrication of iron carbide based nanocomposites. The secondary growth approach through decomposition or reduction of the metal precursor at low temperature had led to a core-shell or core-satellite structure of FeC_x-M. The FeC_x-M heterostructures combine the advantages of iron carbides and second metals in catalysis. We

anticipate that more of such heterostructures in catalysis shall arise in the future. In general, the development of chemical synthetic strategies of FeC_x can lead to the rational design of versatile FeC_x-based nanohybrids with different structures and compositions.

The development in the synthesis of iron carbides-based nanomaterials has dramatically broadened their catalytic applications. FeC_x is a promising functionalized support for catalysis due to its unique physical properties. The loaded noble metals has been separated and reused readily because of the magnetism of FeC_x. Moreover, FeC_x NPs possess excellent photothermal and magnetothermal properties and therefore could catalyze photo- and magnetic-induced reactions in a closed or even continuous-flow reactor. Particularly, the temperature of these catalysis systems could reach 400 - 500 ^oC when FeC_x NPs were exposed to light or external magnetic field. We anticipate that further investigation of FeC_x as functionalized supports will be carried out for other important industrial reactions, particularly at high temperatures, such as for methane activation, alkane dehydrogenation and ammonia synthesis. A highly promising research field is foreseen to unroll with ample results anticipated from well-designed iron carbides and their applications in heterogeneous catalysis, which will shed light on the role of metal carbides in various catalytic processes.

Acknowledgements

This work was financially supported by the National Natural Science Foundation of China (21725301, 91645115, 21473003, 21872104) and the MOST (2017YFB0602200).

Received: ((will be filled in by the editorial staff))
Revised: ((will be filled in by the editorial staff))
Published online: ((will be filled in by the editorial staff))

References:

[1] L. Lin, W. Zhou, R. Gao, S. Yao, X. Zhang, W. Xu, S. Zheng, Z. Jiang, Q. Yu, Y.-W. Li, C. Shi, X.-D. Wen, D. Ma, *Nature* **2017**, 544, 80.

[2] S. Li, Y. Xu, Y. Chen, W. Li, L. Lin, M. Li, Y. Deng, X. Wang, B. Ge, C. Yang, S. Yao, J. Xie, Y. Li, X. Liu, D. Ma, *Angew. Chem. Int. Ed.* **2017**, 56, 10761.

[3] S. Kattel, P. J. Ramirez, J. G. Chen, J. A. Rodriguez, P. Liu, *Science* **2017**, 355, 1296.
[4] J. Graciani, K. Mudiyanselage, F. Xu, A. E. Baber, J. Evans, S. D. Senanayake, D. J. Stacchiola, P. Liu, J. Hrbek, J. Fernandez Sanz, J. A. Rodriguez, *Science* **2014**, 345, 546.
[5] M. Xu, S. Yao, D. Rao, Y. Niu, N. Liu, M. Peng, P. Zhai, Y. Man, L. Zheng, B. Wang, B. Zhang, D. Ma, M. Wei, *J. Am. Chem. Soc.* **2018**, 140, 11241.
[6] J. Kang, K. Cheng, L. Zhang, Q. Zhang, J. Ding, W. Hua, Y. Lou, Q. Zhai, Y. Wang, *Angew. Chem. Int. Ed.* **2011**, 50, 5200.
[7] F. Jiao, J. Li, X. Pan, J. Xiao, H. Li, H. Ma, M. Wei, Y. Pan, Z. Zhou, M. Li, S. Miao, J. Li, Y. Zhu, D. Xiao, T. He, J. Yang, F. Qi, Q. Fu, X. Bao, *Science* **2016**, 351, 1065.
[8] L. Zhong, F. Yu, Y. An, Y. Zhao, Y. Sun, Z. Li, T. Lin, Y. Lin, X. Qi, Y. Dai, L. Gu, J. Hu, S. Jin, Q. Shen, H. Wang, *Nature* **2016**, 538, 84.
[9] H. T. Luk, C. Mondelli, D. C. Ferre, J. A. Stewart, J. Perez-Ramirez, *Chem. Soc. Rev.* **2017**, 46, 1358.
[10] G. L. Bezemer, J. H. Bitter, H. Kuipers, H. Oosterbeek, J. E. Holewijn, X. D. Xu, F. Kapteijn, A. J. van Dillen, K. P. de Jong, *J. Am. Chem. Soc.* **2006**, 128, 3956.
[11] E. Iglesia, *Appl. Catal. A Gen.* **1997**, 161, 59.
[12] W. Wang, S. Wang, X. Ma, J. Gong, *Chem. Soc. Rev.* **2011**, 40, 3703.
[13] J. C. Matsubu, S. Zhang, L. DeRita, N. S. Marinkovic, J. G. Chen, G. W. Graham, X. Pan, P. Christopher, *Nat. Chem.* **2017**, 9, 120.
[14] X. Zou, Y. Zhang, *Chem. Soc. Rev.* **2015**, 44, 5148.
[15] Y. P. Zhu, C. Guo, Y. Zheng, S.-Z. Qiao, *Acc. Chem. Res.* **2017**, 50, 915.
[16] J. Wang, F. Xu, H. Jin, Y. Chen, Y. Wang, *Adv. Mater.* **2017**, 29.
[17] C. Yang, H. Zhao, Y. Hou, D. Ma, *J. Am. Chem. Soc.* **2012**, 134, 15814.
[18] E. de Smit, F. Cinquini, A. M. Beale, O. V. Safonova, W. van Beek, P. Sautet, B. M. Weckhuysen, *J. Am. Chem. Soc.* **2010**, 132, 14928.
[19] L. C. Browning, P. H. Emmett, *J. Am. Chem. Soc.* **1951**, 73, 581.
[20] L. C. Browning, T. W. Dewitt, P. H. Emmett, *J. Am. Chem. Soc.* **1950**, 72, 4211.
[21] S. Janbroers, J. N. Louwen, H. W. Zandbergen, P. J. Kooyman, *J. Catal.* **2009**, 268, 235.
[22] D. B. Bukur, K. Okabe, M. P. Rosynek, C. P. Li, D. J. Wang, K. Rao, G. P. Huffman, *J. Catal.* **1995**, 155, 353.
[23] R. J. P. Broos, B. Zijlstra, I. A. W. Filot, E. J. M. Hensen, *J. Phys. Chem. C* **2018**, 122, 9929.
[24] T. A. Wezendonk, X. Sun, A. I. Dugulan, A. J. F. van Hoof, E. J. M. Hensen, F. Kapteijn, J. Gascon, *J. Catal.* **2018**, 362, 106.
[25] P. Zhai, C. Xu, R. Gao, X. Liu, M. Li, W. Li, X. Fu, C. Jia, J. Xie, M. Zhao, X. Wang, Y.-W. Li, Q. Zhang, X.-D. Wen, D. Ma, *Angew. Chem. Int. Ed.* **2016**, 55, 9902.
[26] B. Zhao, P. Zhai, P. Wang, J. Li, T. Li, M. Peng, M. Zhao, G. Hu, Y. Yang, Y.-W. Li, Q. Zhang, W. Fan, D. Ma, *Chem* **2017**, 3, 323.
[27] H. M. Torres Galvis, J. H. Bitter, C. B. Khare, M. Ruitenbeek, A. I. Dugulan, K. P. de Jong, *Science* **2012**, 335, 835.

[28] J. Wei, Q. Ge, R. Yao, Z. Wen, C. Fang, L. Guo, H. Xu, J. Sun, *Nat. Commun.* **2017**, 8, 15174.
[29] L. Xiao, Z. Wen, S. Ci, J. Chen, Z. He, *Nano Energy* **2012**, 1, 751.
[30] X. Fan, Z. Peng, R. Ye, H. Zhou, X. Guo, *ACS Nano* **2015**, 9, 7407.
[31] Z. Wen, S. Ci, F. Zhang, X. Feng, S. Cui, S. Mao, S. Luo, Z. He, J. Chen, *Adv. Mater.* **2012**, 24, 1399.
[32] J. Lai, B. Huang, Y. Tang, F. Lin, P. Zhou, X. Chen, Y. Sun, F. Lv, S. Guo, *Chem* **2018**, 4, 1153.
[33] Y. Hou, T. Huang, Z. Wen, S. Mao, S. Cui, J. Chen, *Adv. Energy Mater.* **2014**, 4, 140337.
[34] W.-J. Jiang, L. Gu, L. Li, Y. Zhang, X. Zhang, L.-J. Zhang, J.-Q. Wang, J.-S. Hu, Z. Wei, L.-J. Wan, *J. Am. Chem. Soc.* **2016**, 138, 3570.
[35] Z.-Y. Wu, X.-X. Xu, B.-C. Hu, H.-W. Liang, Y. Lin, L.-F. Chen, S.-H. Yu, *Angew. Chem. Int. Ed.* **2015**, 54, 8179.
[36] M. Zhou, H.-L. Wang, S. Guo, *Chem. Soc. Rev.* **2016**, 45, 1273.
[37] J. Jia, H. Yang, G. Wang, P. Huang, P. Cai, Z. Wen, *ChemElectroChem* **2018**, 5, 471.
[38] C. Giordano, A. Kraupner, S. C. Wimbush, M. Antonietti, *Small* **2010**, 6, 1859.
[39] S. I. Hirano, S. Tajima, *J. Mater. Sci.* **1990**, 25, 4457.
[40] W. Yang, S. Rehman, X. Chu, Y. Hou, S. Gao, *ChemNanoMat* **2015**, 1, 376.
[41] J. Chipman, *Metall. Trans.* **1972**, 3, 55.
[42] W. Gao, R. Gao, Y. Zhao, M. Peng, C. Song, M. Li, S. Li, J. Liu, W. Li, Y. Deng, M. Zhang, J. Xie, G. Hu, Z. Zhang, R. Long, X.-D. Wen, D. Ma, *Chem* **2018**, 4, 2917.
[43] Z. Schnepp, S. C. Wimbush, M. Antonietti, C. Giordano, *Chem. Mater.* **2010**, 22, 5340.
[44] B. Williams, D. Clifford, A. A. El-Gendy, E. E. Carpenter, *J. Appl. Phys.* **2016**, 120.
[45] J. Yu, Y. Ju, L. Zhao, X. Chu, W. Yang, Y. Tian, F. Sheng, J. Lin, F. Liu, Y. Dong, Y. Hou, *ACS Nano* **2016**, 10, 159.
[46] J. Yu, C. Yang, J. Li, Y. Ding, L. Zhang, M. Z. Yousaf, J. Lin, R. Pang, L. Wei, L. Xu, F. Sheng, C. Li, G. Li, L. Zhao, Y. Hou, *Adv. Mater.* **2014**, 26, 4114.
[47] Y. Ju, H. Zhang, J. Yu, S. Tong, N. Tian, Z. Wang, X. Wang, X. Su, X. Chu, J. Lin, Y. Ding, G. Li, F. Sheng, Y. Hou, *ACS Nano* **2017**, 11, 9239.
[48] C. Giordano, C. Erpen, W. Yao, M. Antoniett, *Nano Lett.* **2008**, 8, 4659.
[49] C. Giordano, M. Antonietti, *Nano Today* **2011**, 6, 366.
[50] C. Giordano, A. Kraupner, I. Fleischer, C. Henrich, G. Klingelhoefer, M. Antonietti, *J. Mater. Chem.* **2011**, 21, 16963.
[51] A. Hanif, T. Xiao, A. P. E. York, J. Sloan, M. L. H. Green, *Chem. Mater.* **2002**, 14, 1009.
[52] X. Liu, C. Zhang, Y. Li, J. W. Niemantsverdriet, J. B. Wagner, T. W. Hansen, *ACS Catal.* **2017**, 7, 4867.
[53] Z. Ye, P. Zhang, X. Lei, X. Wang, N. Zhao, H. Yang, *Chem. Euro. J* **2018**, 24, 8922.
[54] O. Malina, P. Jakubec, J. Kašlík, J. Tuček, R. Zbořil, *Nanoscale* **2017**, 9, 10440.
[55] P. Wang, W. Chen, F.-K. Chiang, A. I. Dugulan, Y. Song, R. Pestman, K. Zhang, J. Yao, B. Feng, P. Miao, W. Xu, E. J. M. Hensen, *Sci. Adv.* **2018**, 4, 2947.

[56] Z. Xu, Y. Du, D. Liu, Y. Wang, W. Ma, Y. Wang, P. Xu, X. Han, *ACS Appl. Mater. Interfaces* **2019**, 11, 4268.

[57] Y. Hu, J. O. Jensen, W. Zhang, L. N. Cleemann, W. Xing, N. J. Bjerrum, Q. Li, *Angew. Chem. Int. Ed.* **2014**, 53, 3675.

[58] W. Yang, X. Liu, X. Yue, J. Jia, S. Guo, *J. Am. Chem. Soc.* **2015**, 137, 1436.

[59] S. H. Sun, H. Zeng, D. B. Robinson, S. Raoux, P. M. Rice, S. X. Wang, G. X. Li, *J. Am. Chem. Soc.* **2004**, 126, 273.

[60] Y. Hou, Z. Xu, S. Sun, *Angew. Chem. Int. Ed.* **2007**, 46, 6329.

[61] A. Meffre, B. Mehdaoui, V. Kelsen, P. F. Fazzini, J. Carrey, S. Lachaize, M. Respaud, B. Chaudret, *Nano Lett.* **2012**, 12, 4722.

[62] S. Yao, C. Yang, H. Zhao, S. Li, L. Lin, W. Wen, J. Liu, G. Hu, W. Li, Y. Hou, D. Ma, *J. Phys. Chem. C* **2017**, 121, 5154.

[63] S. Li, C. Yang, Z. Yin, H. Yang, Y. Chen, L. Lin, M. Li, W. Li, G. Hu, D. Ma, *Nano Res.* **2017**, 10, 1322.

[64] Z. Yang, T. Zhao, X. Huang, X. Chu, T. Tang, Y. Ju, Q. Wang, Y. Hou, S. Gao, *Chem. Sci.* **2017**, 8, 473.

[65] S. Li, P. Ren, C. Yang, X. Liu, Z. Yin, W. Li, H. Yang, J. Li, X. Wang, Y. Wang, R. Cao, L. Lin, S. Yao, X. Wen, D. Ma, *Sci. Bull.* **2018**, 63, 1358.

[66] C. Yang, B. Zhao, R. Gao, S. Yao, P. Zhai, S. Li, J. Yu, Y. Hou, D. Ma, *ACS Catal.* **2017**, 7, 5661.

[67] A. Bordet, L.-M. Lacroix, P.-F. Fazzini, J. Carrey, K. Soulantica, B. Chaudret, *Angew. Chem. Int. Ed.* **2016**, 55, 15894.

[68] K. Cheng, M. Virginie, V. V. Ordomsky, C. Cordier, P. A. Chernavskii, M. I. Ivantsov, S. Paul, Y. Wang, A. Y. Khodakov, *J. Catal.* **2015**, 328, 139.

[69] V. P. Santos, T. A. Wezendonk, J. J. Delgado Jaen, A. I. Dugulan, M. A. Nasalevich, H.-U. Islam, A. Chojecki, S. Sartipi, X. Sun, A. A. Hakeem, A. C. J. Koeken, M. Ruitenbeek, T. Davidian, G. R. Meima, G. Sankar, F. Kapteijn, M. Makkee, J. Gascon, *Nat. Commun.* **2015**, 6, 6451.

[70] E. de Smit, B. M. Weckhuysen, *Chem. Soc. Rev.* **2008**, 37, 2758.

[71] E. de Smit, A. M. Beale, S. Nikitenko, B. M. Weckhuysen, *J. Catal.* **2009**, 262, 244.

[72] T. Herranz, S. Rojas, F. J. Perez-Alonso, M. Ojeda, P. Terreros, J. L. G. Fierro, *J. Catal.* **2006**, 243, 199.

[73] E. Boellaard, A. M. VanderKraan, J. W. Geus, *Appl. Catal. A Gen.* **1996**, 147, 229.

[74] J. W. Niemantsverdriet, A. M. Vanderkraan, W. L. Vandijk, H. S. Vanderbaan, *J. Phys. Chem.* **1980**, 84, 3363.

[75] G. B. Raupp, W. N. Delgass, *J. Catal.* **1979**, 58, 348.

[76] K. Xu, B. Sun, J. Lin, W. Wen, Y. Pei, S. Yan, M. Qiao, X. Zhang, B. Zong, *Nat. Commun.* **2014**, 5, 5783.

[77] Q. Chang, C. Zhang, C. Liu, Y. Wei, A. V. Cheruvathur, A. I. Dugulan, J. W. Niemantsverdriet, X. Liu, Y. He, M. Qing, L. Zheng, Y. Yun, Y. Yang, Y. Li, *ACS Catal.* **2018**, 8, 3304.

[78] H. M. T. Galvis, J. H. Bitter, T. Davidian, M. Ruitenbeek, A. I. Dugulan, K. P. de Jong, *J Am. Chem. Soc.* **2012**, 134, 16207.

[79] E. de Smit, F. Cinquini, A. M. Beale, O. V. Safonova, W. van Beek, P. Sautet, B. M. Weckhuysen, *J. Am. Chem. Soc.* **2010**, 132, 14928.

[80] E. de Smit, B. M. Weckhuysen, *Chem. Soc. Rev.* **2008**, 37, 2758.

[81] O. Borg, P. D. C. Dietzel, A. I. Spjelkavik, E. Z. Tveten, J. C. Walmsley, S. Diplas, S. Eri, A. Holmen, E. Ryttera, *J. Catal.* **2008**, 259, 161.

[82] J. P. den Breejen, J. R. A. Sietsma, H. Friedrich, J. H. Bitter, K. P. de Jong, *J. Catal.* **2010**, 270, 146.

[83] G. L. Bezemer, J. H. Bitter, H. P. C. E. Kuipers, H. Oosterbeek, J. E. Holewijn, X. D. Xu, F. Kapteijn, A. J. van Dillen, K. P. de Jong, *J. Am. Chem. Soc.* **2006**, 128, 3956.

[84] Z. Yan, Z. J. Wang, D. B. Bukur, D. W. Goodman, *J. Catal.* **2009**, 268, 196.

[85] A. Y. Khodakov, W. Chu, P. Fongarland, *Chem. Rev.* **2007**, 107, 1692.

[86] M. D. Porosoff, B. Yan, J. G. Chen, *Energy Environ. Sci.* **2016**, 9, 62.

[87] S. Saeidi, S. Najari, F. Fazlollahi, M. K. Nikoo, F. Sefidkon, J. J. Klemes, L. L. Baxter, *Renew. Sust. Energ. Rev.* **2017**, 80, 1292.

[88] Y. Gao, S. Liu, Z. Zhao, H. Tao, Z. Sun, *Acta Phys. Chim. Sin.* **2018**, 34, 858.

[89] R. W. Dorner, D. R. Hardy, F. W. Williams, H. D. Willauer, *Catal. Commun.* **2011**, 15, 88.

[90] Y. H. Choi, Y. J. Jang, H. Park, W. Y. Kim, Y. H. Lee, S. H. Choi, J. S. Lee, *Appl. Catal. B Environ.* **2017**, 202, 605.

[91] M. Rafati, L. Wang, A. Shahbazi, *J. CO_2 Util.* **2015**, 12, 34.

[92] C. G. Visconti, M. Martinelli, L. Falbo, A. Infantes-Molina, L. Lietti, P. Forzatti, G. Iaquaniello, E. Palo, B. Picutti, F. Brignoli, *Appl. Catal. B Environ.* **2017**, 200, 530.

[93] H. Schulz, *Appl. Catal. A Gen.* **1999**, 186, 3.

[94] C.-x. Xiao, Z.-p. Cai, T. Wang, Y. Kou, N. Yan, *Angew. Chem. Int. Ed.* **2008**, 47, 746.

[95] C. Niether, S. Faure, A. Bordet, J. Deseure, M. Chatenet, J. Carrey, B. Chaudret, A. Rouet, *Nat. Chem.* **2018**, 3, 476.

[96] Y. Zhao, B. Zhao, J. Liu, G. Chen, R. Gao, S. Yao, M. Li, Q. Zhang, L. Gu, J. Xie, X. Wen, L.-Z. Wu, C.-H. Tung, D. Ma, T. Zhang, *Angew. Chem. Int. Ed.* **2016**, 55, 4215.

[97] F. Sastre, A. V. Puga, L. Liu, A. Corma, H. Garcia, *J. Am. Chem. Soc.* **2014**, 136, 6798.

[98] S. Ceylan, C. Friese, C. Lammel, K. Mazac, A. Kirschning, *Angew. Chem. Int. Ed.* **2008**, 47, 8950.

[99] J. Hartwig, S. Ceylan, L. Kupracz, L. Coutable, A. Kirschning, *Angew. Chem. Int. Ed.* **2013**, 52, 9813.

[100] E. V. Kondratenko, G. Mul, J. Baltrusaitis, G. O. Larrazabal, J. Perez-Ramirez, *Energy Environ. Sci.* **2013**, 6, 3112.

[101] Q. Gao, W. Zhang, Z. Shi, L. Yang, Y. Tang, *Adv. Mater.* **2019**, 31, e1802880.

[102] D. V. Esposito, S. T. Hunt, A. L. Stottlemyer, K. D. Dobson, B. E. McCandless, R. W. Birkmire, J. G. Chen, *Angew. Chem. Int. Ed.* **2010**, 49, 9859.

[103] C. Wan, Y. N. Regmi, B. M. Leonard, *Angew. Chem. Int. Ed.* **2014**, 53, 6407.

[104] C. Lv, Q. Yang, Q. Huang, Z. Huang, H. Xia, C. Zhang, *J. Mater. Chem. A* **2016**, 4, 13336.

[105] H. Lin, W. Zhang, Z. Shi, M. Che, X. Yu, Y. Tang, Q. Gao, *ChemSusChem* **2017**, 10, 2597.

[106] F. Kong, X. Fan, A. Kong, Z. Zhou, X. Zhang, Y. Shan, *Adv. Funct. Mater.* **2018**, 28.

[107] L. Zhang, Y. Chen, P. Zhao, W. Luo, S. Chen, M. Shao, *Electrocatalysis* **2018**, 9, 264.

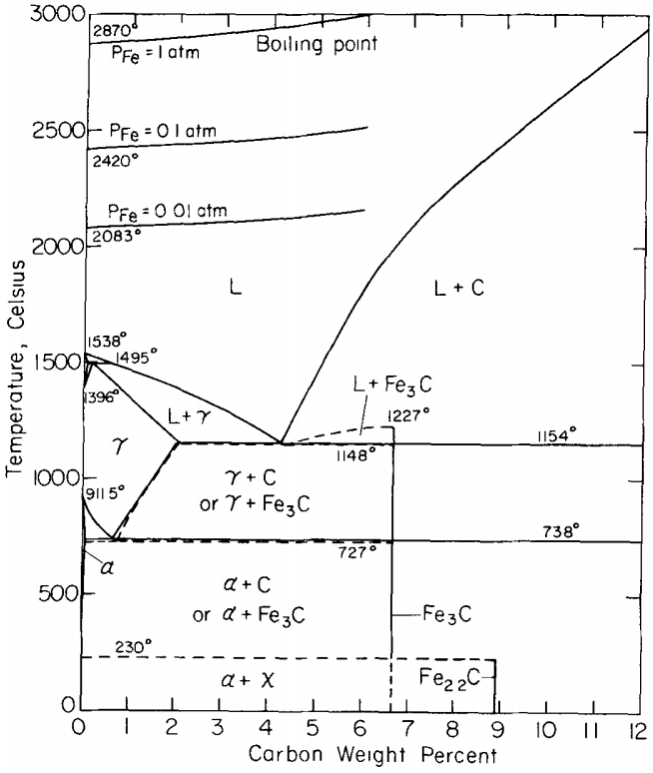

Figure 1. The Fe-C phase diagram. Copyright 1972, Springer.[41]

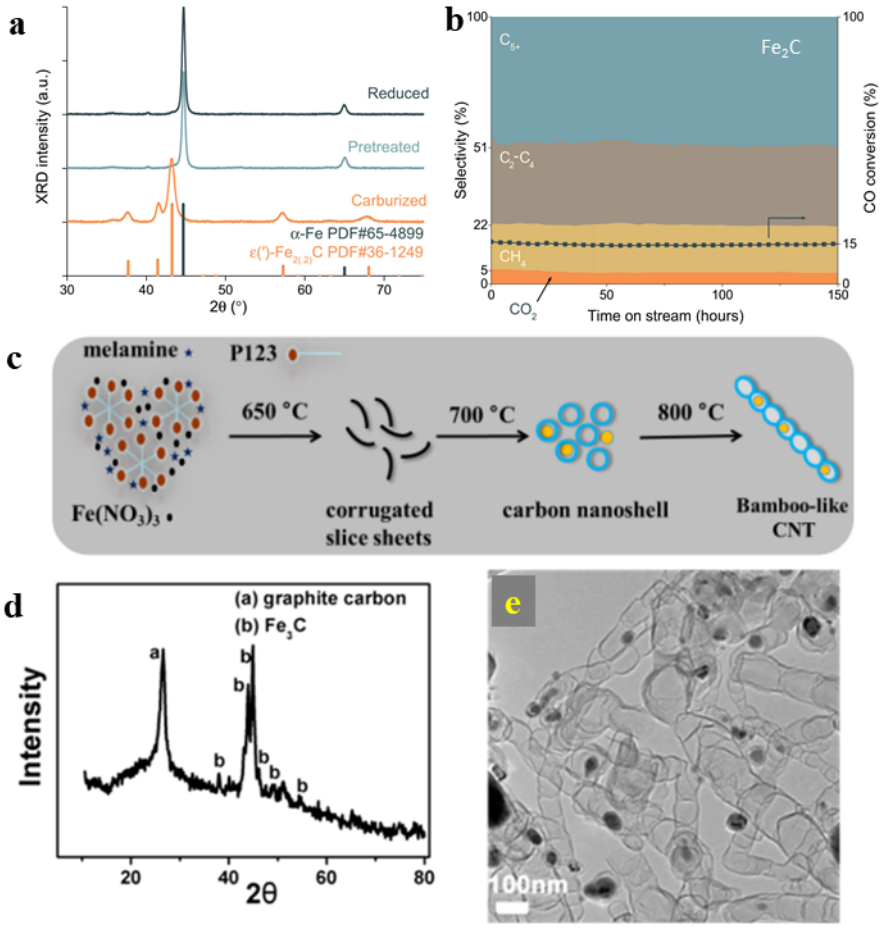

Figure 2. Synthesis of iron carbides via solid-state reaction methods. (a) XRD patterns of Fe_2C catalyst and the synthetic intermediates. (b) FT performance of the Fe_2C catalyst. Reaction conditions: CO/H_2 = 2/3, 2.3 MPa, 235°C, GHSV of 18,000 $hour^{-1}$. Copyright 2018, Science AAAS.[55] (c) Schematic illustration of the synthesis of carbon nanotube/Fe_3C electrocatalyst. (d) XRD patterns and (e) TEM images of the nanostructures. Copyright 2015, American Chemical Society.[58]

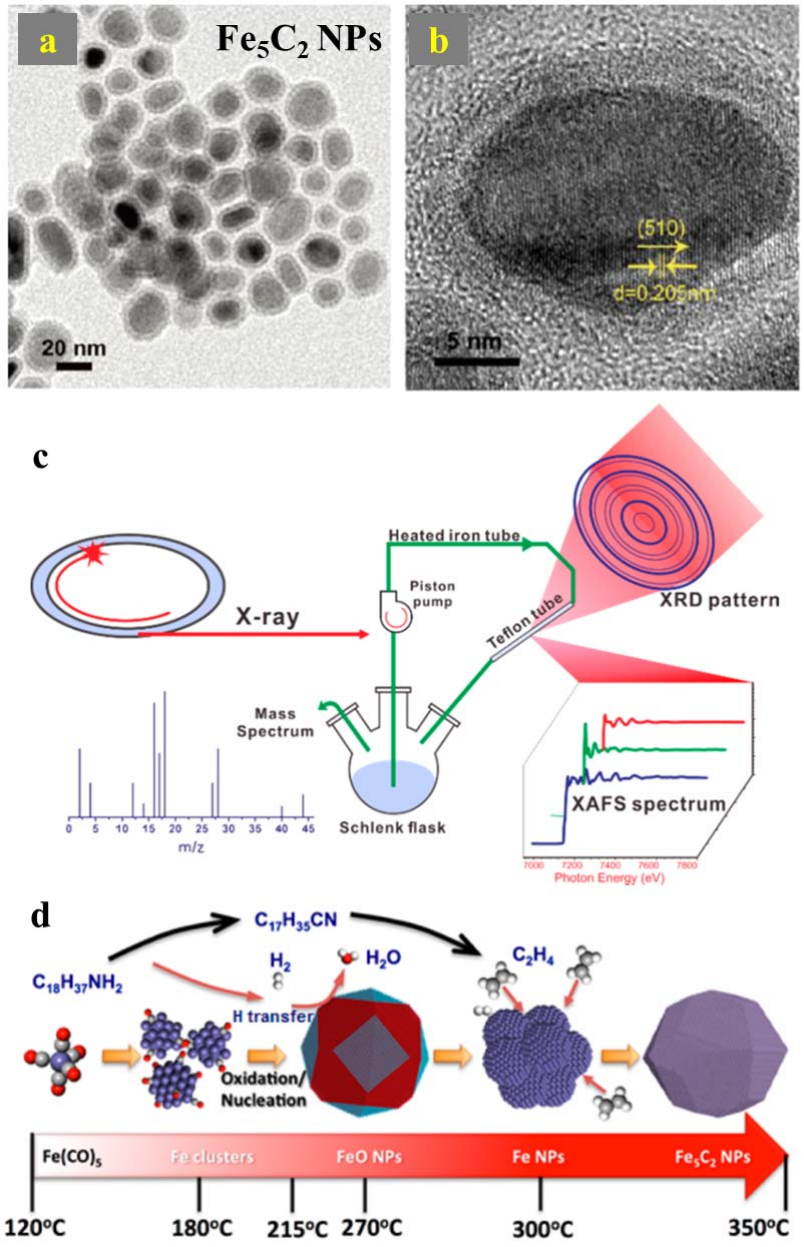

Figure 3. Wet chemical synthesis of Fe_5C_2 NPs. (a) TEM and (b) HRTEM images of the Fe_5C_2 NPs. Copyright 2012, American Chemical Society.[17] (c) Schematic illustration of home-made circulate apparatus for operando investigation of wet chemical synthesis. (d) Schematic illustration of evolution of NPs and solvent during the synthetic reaction of Fe_5C_2. Copyright 2017, American Chemical Society.[62]

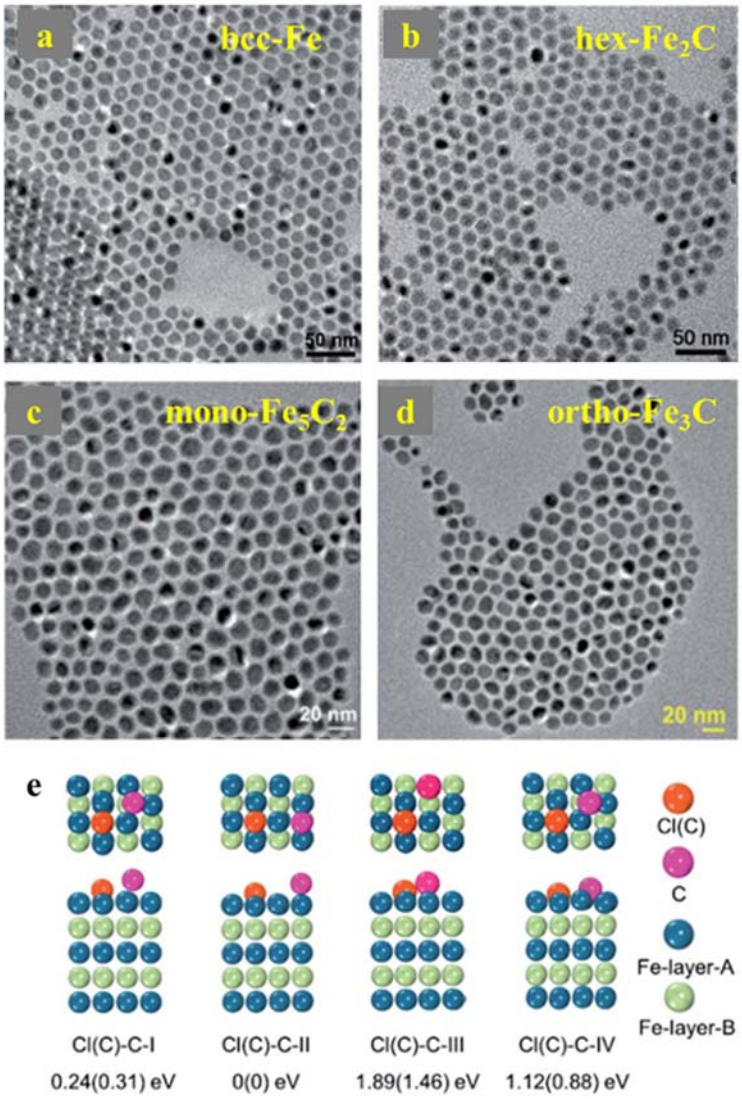

Figure 4. Phase control of iron carbides NPs via seeded-growth method. TEM images of (a) bcc-Fe@Fe_3O_4 seeds, (b) hex-Fe_2C NPs, (c) mono-Fe_5C_2 NPs and (d) ortho-Fe_3C NPs. (e) The adsorption configurations of the second C atom on the Fe surface that has already adsorbed a Cl or C atom. Copyright 2016, Royal Society of Chemistry.[64]

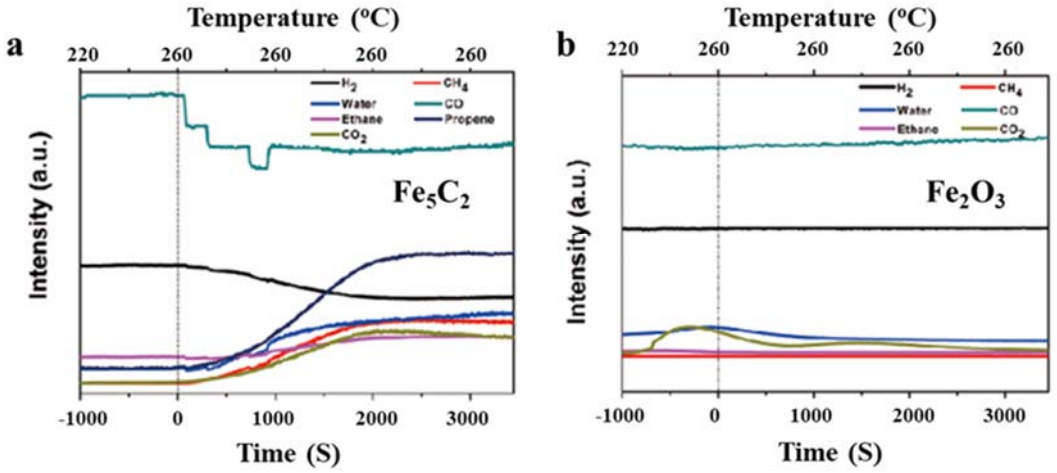

Figure 5. Temperature and time dependent temperature programmed surface reaction diagrams for (a) Fe_5C_2 and (b) Fe_2O_3 catalysts. Reproduced with Copyright 2012, American Chemical Society.[17]

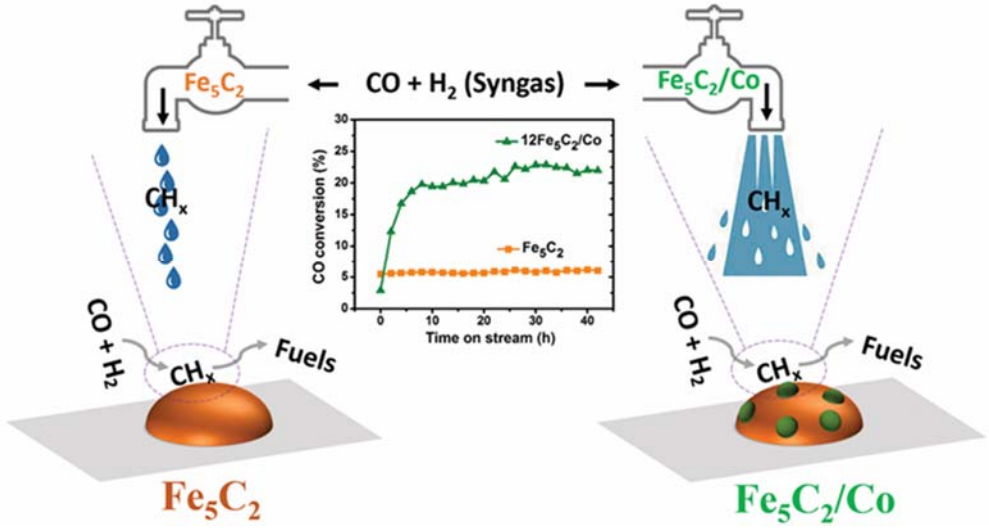

Figure 6. Schematic illustration of the Fe_5C_2 and Fe_5C_2/Co catalysts in low temperature FTS. Reaction conditions: 3MPa, 220 °C, and GHSV=15,000 $cm^3\ h^{-1}g_{cat}^{-1}$. Copyright 2017, American Chemical Society.[66]

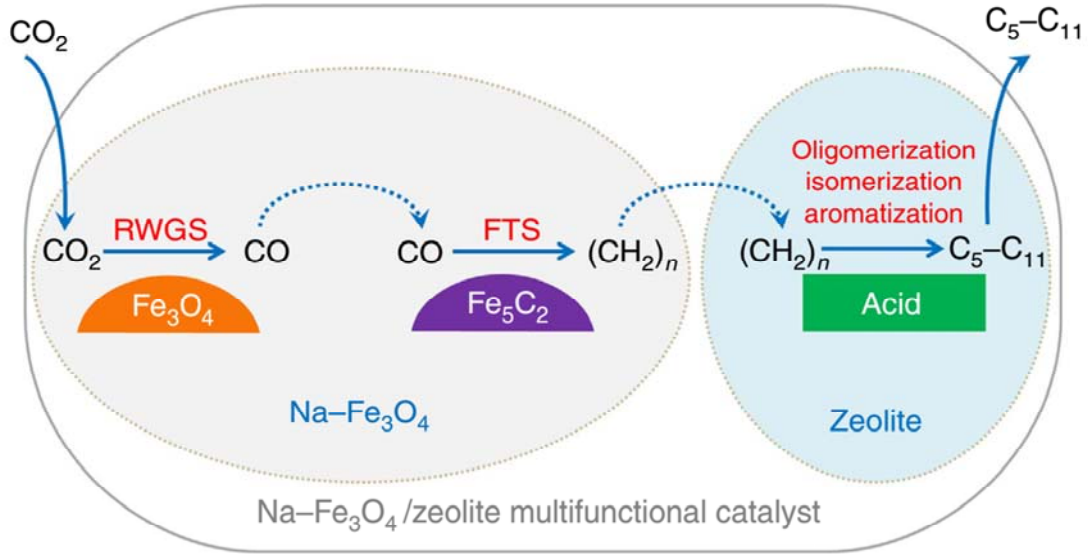

Figure 7. Schematic illustration for CO_2 hydrogenation to gasoline-range hydrocarbons over Na–Fe_3O_4/Zeolite catalyst. Copyright 2017, Springer Nature. [28]

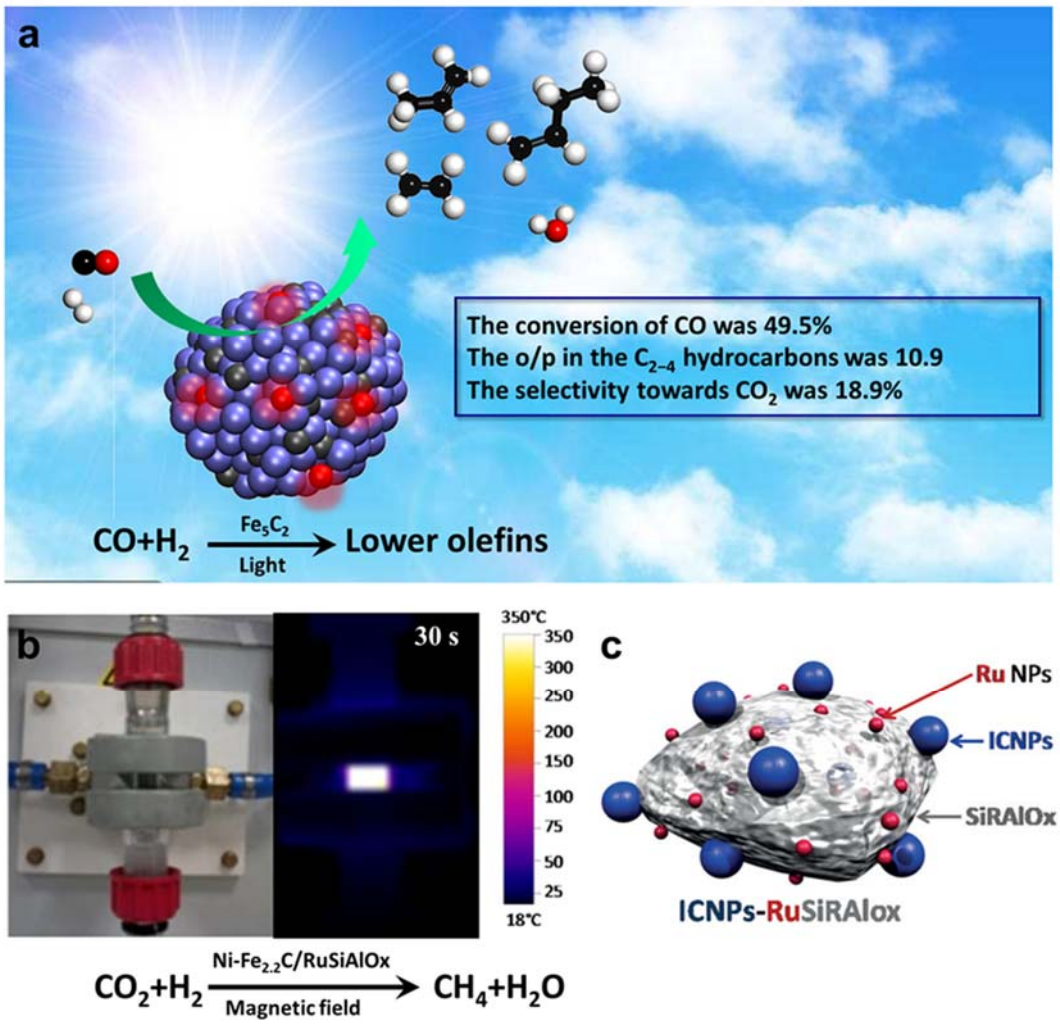

Figure 8. CO_x transformation with renewable energy over iron carbides catalysts. (a) Schematic illustration of the photo-driven CO hydrogenation to olefins over Fe_5C_2 catalysts. Copyright 2018, Elsevier.[42] (b) Magnetism-induced CO_2 methanation reaction over Ni-$Fe_{2.2}C$/$RuSiAlO_x$ catalysts. Thermal images of the reactor exposed to the alternating magnetic field (64 mT, 300 kHz). (c) Schematic representation of the FeC_x-based catalysts. Copyright 2016, Wiley-VCH.[67]

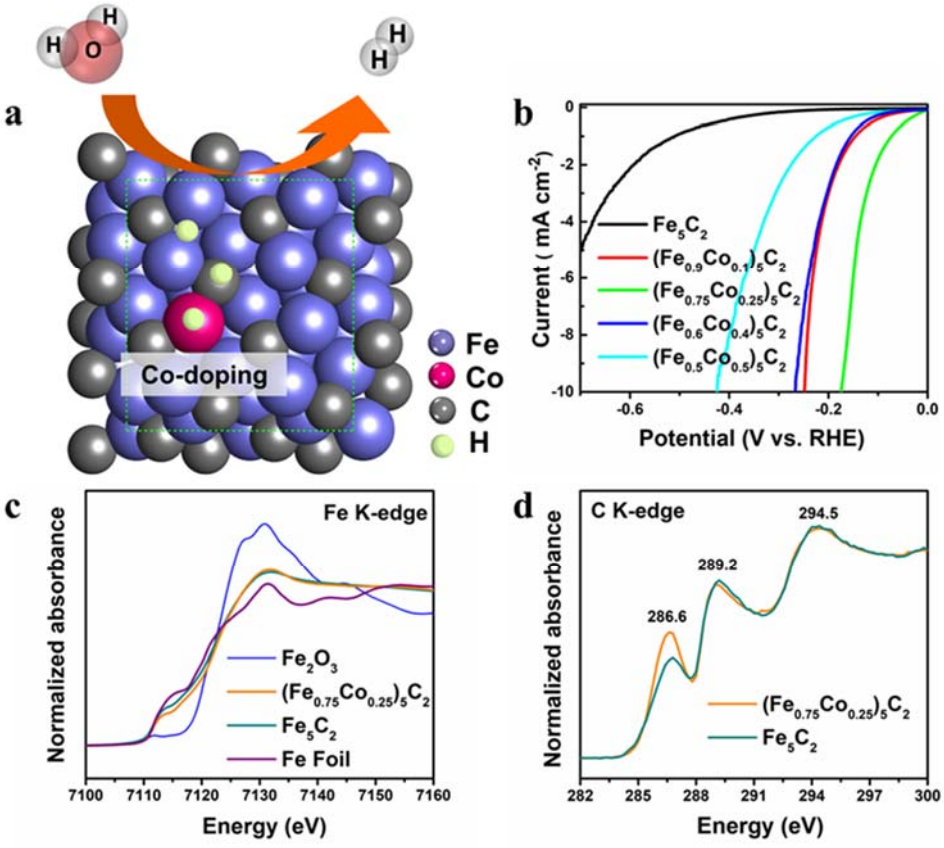

Figure 9. (a) Schematic illustration of electrocatalytic HER over Co-modified Fe_5C_2 NPs. (b) Polarization curves obtained over the $(Fe_{1-x}Co_x)_5C_2$ NPs with different Co content; (c) Fe K-edge XANES and (d) C K-edge XAS of $(Fe_{0.75}Co_{0.25})_5C_2$ and Fe_5C_2 electrocatalysts. Copyright 2018, Elsevier.[65]